Innovative tools for offshore wind and DC grids

Deliverable 1.2 – Work Package 1
Report on the control requirements, protections and fault management of DC/DC converters and MMCs

Dissemination level	Public
Website	http://innodc.org/
Grant Agreement number	765585
Due delivery	Month 18 - 28 Feb 2018
Project dates	01/09/2017 – 31/08/2021

Authors	**Names**
ESR1	Peng Yang
ESR4	Davide Pinzan
ESR5	Daniel Westerman Spier
ESR12	Stephen Hardy
ESR14	Motaz Ayiad
WP1 leader	Eduardo Prieto-Araujo

Summary

This deliverable contains a summary of the research developed by Work Package 1 researchers within InnoDC project. It contains an analysis on the control requirements, protections and fault management of MMC-based AC/DC and DC/DC converters for HVDC grids.

As a basic unit for HVDC converters, a brief description of the Modular Multilevel Converter (MMC) is given and the mathematical description of the topology is explained. Based on it, a steady state analysis is performed for a better understanding of the behavior of the converter, detailing the current uses within the structure and its control requirements. Then, an energy-based MMC control strategy is detailed for a conventional AC/DC operation mode.

Aligned with the ongoing project research, the analysis of the DC/DC converter included in the deliverable is focused on the MMC Dual Active Bridge (MMC-DAB), assumed as a reference DC/DC topology. Based on the previous MMC description, the control requirements are focused on the power transfer between both MMCs also detailing an example control strategy. In addition, simulations and experiments of a two-level DAB are presented to verify the suggested control strategy.

Furthermore, the MMC and DC/DC protection systems for HVDC applications are introduced. The converter protection description is divided between the AC and DC sides of the converter, also including the converter internal and transformer protections.

An overview of surge arresters for overvoltage protection in HVDC substations is given and the consequences of their dimensioning are discussed. Finally, the Supervisory Control and Data Acquisition aspect is described, providing an explanation of its functions for HVDC grids.

Contents

1 The Modular Multilevel Converter

The Modular Multilevel Converter (MMC) is the base converter topology used in HVDC grids. Multilevel structures are required to withstand the high voltages presents at both sides of the converter. Currently, MMC converters are being used to interconnect AC and DC networks, but this topology can be further used as part of the future DC/DC converters that will be installed in HVDC networks. The MMC analysis is performed following the procedure described in [1],[2].

1.1 MMC converter topology

The three-phase modular multilevel converter (MMC) circuit is presented in Fig. 1. It consists of three legs, one per phase, in which each leg has two arms with N_{arm} sub-modules (SM) connected in series and two arm inductances L_{arm}. The SMs can be regulated separately to either connect the capacitor voltage in series with the arm or to bypass it; thus, the arms can behave as controlled voltage sources[1] [3]. By setting the proper values for the currents circulating across the converter, it is possible to achieve the desired power exchange between the AC and the DC grids and, at the same time, to keep its internal energy balanced [1].

Next, the mathematical model of the MMC converter is detailed in order to illustrate the different degrees of freedom and control requirements of the converter. The mathematical description is be obtained per phase j ($j = a, b, c$) [4] as

$$V_u^{DC} - v_u^j - v_g^j - v_n = R_a i_u^j + L_a \frac{di_u^j}{dt} + R_s i_s^j + L_s \frac{di_s^j}{dt} \tag{1}$$

$$-V_l^{DC} + v_l^j - v_g^j - v_n = -R_a i_l^j - L_a \frac{di_l^j}{dt} + R_s i_s^j + L_s \frac{di_s^j}{dt} \tag{2}$$

where V_u^{DC} and V_l^{DC} are the voltages of the upper and the lower halves of the HVDC link, v_u^j and v_l^j are the voltages applied by the upper and the lower arms respectively, v_g^j is the AC grid voltage, R_a and L_a are the resistance and inductance of the arm inductor respectively, R_s and L_s correspond to the phase inductor, i_u^j and i_l^j are the currents flowing through the upper

[1]MMC modulation techniques for voltage application are described in appendix A.

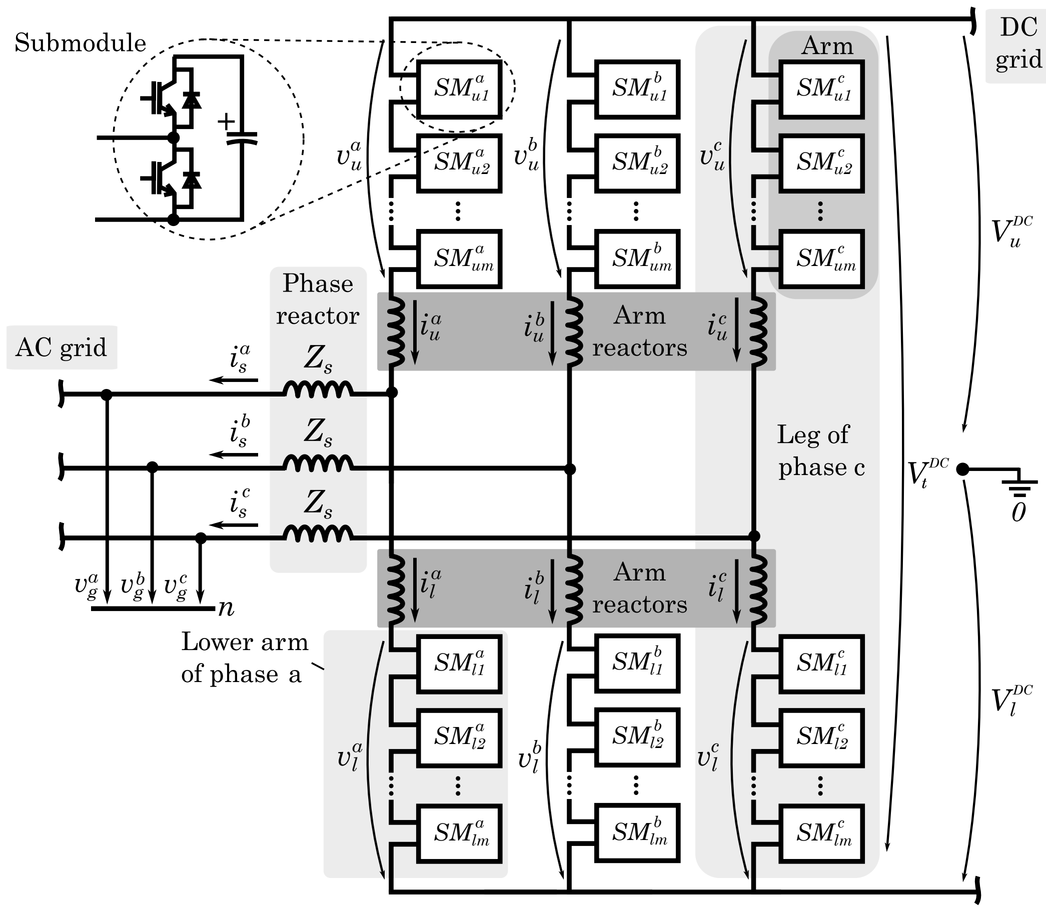

Figure 1: Complete scheme of the Modular Multilevel Converter.

and lower arms respectively and i_s^j is the AC grid current. Typically, MMC equations are expressed in a different domain, to facilitate the understanding of the converter. These variables are defined as follows [2]

$$\begin{cases} v_{diff}^j \triangleq \dfrac{1}{2}(-v_u^j + v_l^j) \\ v_{sum}^j \triangleq v_u^j + v_l^j \\ i_{sum}^j \triangleq \dfrac{1}{2}(i_u^j + i_l^j) \\ R \triangleq R_s + \dfrac{R_a}{2} \\ L \triangleq L_s + \dfrac{L_a}{2} \end{cases} \quad \text{and} \quad \begin{cases} v_u^j = -v_{diff}^j + \dfrac{1}{2} v_{sum}^j \\ v_l^j = v_{diff}^j + \dfrac{1}{2} v_{sum}^j \\ i_u^j = \dfrac{1}{2} i_s^j + i_{sum}^j \\ i_l^j = -\dfrac{1}{2} i_s^j + i_{sum}^j \end{cases} \tag{3}$$

where v_{diff}^j and v_{sum}^j are the differential and the additive voltages applied by the converter respectively and i_{sum}^j is the additive (inner) current, which is common to the upper and lower arms. Thus, applying the transformations in (3), adding and subtracting equations (1) and (2), and then considering that all three phases are symmetric, it is possible to obtain the average equations of the MMC

$$v_{diff}^{abc} - v_g^{abc} + (V_{off}^{DC} - v_n)\begin{bmatrix}1 & 1 & 1\end{bmatrix}^T = \mathbf{R}\, i_s^{abc} + \mathbf{L}\,\frac{di_s^{abc}}{dt} \tag{4}$$

$$v_{sum}^{abc} - V_t^{DC}\begin{bmatrix}1 & 1 & 1\end{bmatrix}^T = -2\mathbf{R_a} i_{sum}^{abc} - 2\mathbf{L_a}\frac{di_{sum}^{abc}}{dt} \tag{5}$$

where V_{off}^{DC} is half the imbalance between the voltage of positive and the negative HVDC poles. This will normally be close to zero but can be large under pole-to-ground faults in the HVDC grid. Also, note that (4) is related to AC side current i_s^j, whereas (5) is related to additive currents i_{sum}^j. Moreover, $\mathbf{R}$, $\mathbf{R_a}$, $\mathbf{L}$ and $\mathbf{L_a}$ are 3×3 diagonal matrices with R, R_a, L and L_a terms at the diagonal, respectively.

Next, a steady-state analysis of the converter is developed in order to understand how the converter currents can be controlled. This analysis will also reveal the converter degrees of freedom and the main uses of current components in the converter.

1.2 Steady-State Analysis

From the previous equations, it could be observed that the MMC deals with AC and DC variables simultaneously. Specific power exchange functions can be assigned to these components to ensure the power flow between AC and DC networks together with an internal energy balancing of the converter. The following analysis decouples the AC terms from the DC ones to detail a comprehensive description of those variables.

1.2.1 AC current components analysis

Expressing equation (4) in AC phasor form[2], it can be rewritten as

$$\underline{V}_{diff}^{abc} - \underline{V}_{g}^{abc} - \underline{V}_{n}\begin{bmatrix}1 & 1 & 1\end{bmatrix}^{T} = \underline{\mathbf{Z}}\,\underline{I}_{s}^{abc} \tag{6}$$

where $\underline{\mathbf{Z}}$ is a 3×3 diagonal matrix with the term $R+j\omega L$ at the diagonal[3]. It is convenient to apply the Fortescue transformation to the previous equation [5]. The Fortescue transformation $\underline{\Theta}^{+-0}$ of a phasor vector $\underline{\Theta}^{abc}$ is defined as

$$\underline{\Theta}^{+-0} \triangleq \mathbf{F}\underline{\Theta}^{abc} = \frac{1}{3}\begin{bmatrix}1 & \alpha & \alpha^2 \\ 1 & \alpha^2 & \alpha \\ 1 & 1 & 1\end{bmatrix}\underline{\Theta}^{abc} \tag{7}$$

with $\alpha = e^{j\frac{2\pi}{3}}$. Multiplying equation (6) by $\mathbf{F}$ leads to

$$\underline{I}_{s}^{+-} = \underline{Z}^{-1}\left[\underline{V}_{diff}^{+-} - \underline{V}_{g}^{+-}\right] \tag{8}$$

Assuming three-wire connection of the AC grid[4], the zero sequence component of the grid current can be extracted from the equation. On the other hand, from (8) it can be concluded that the positive and negative components of this current can be used to exchange power with the AC grid and can be regulated using the differential voltage $\underline{V}_{diff}^{+-}$. The same analysis can be done for additive current, yielding

$$\underline{I}_{sum}^{+-0} = -\frac{1}{2\underline{Z}_{a}}\underline{V}_{sum}^{+-0} \tag{9}$$

The positive and negative sequence components of the additive current (circulating current) $\underline{I}_{sum}^{+-}$ can be controlled applying additive voltage $\underline{V}_{sum}^{+-}$. Both components can be combined to balance the energy differences between the upper and lower halves of the converter. Otherwise, the zero component must be regulated to zero to avoid sending 50 Hz currents to the DC network.

[2]Assuming that V_{off}^{DC} is purely DC it is excluded from the equation

[3]ω is the grid frequency

[4]Different grounding schemes might provide a path for AC zero sequence currents. In this case, a complete analysis of the zero sequence component should be developed.

1.2.2 DC current components analysis

In this section, the DC current components of both the grid and additive currents are studied. As in the AC case, it is interesting to separate the zero sequence component from the other current components. For the grid current, this can be done setting the derivatives to zero and using Clarke transformation [6], defined as

$$\Theta^{\alpha\beta 0} \triangleq \mathbf{C}\Theta^{abc} = \frac{1}{3}\begin{bmatrix} 2 & -1 & -1 \\ 0 & -\sqrt{3} & \sqrt{3} \\ 1 & 1 & 1 \end{bmatrix} \Theta^{abc} \tag{10}$$

Applying (10) to (4), the DC component of the grid current can be expressed as

$$V_{diff}^{\alpha\beta DC} = R\, I_s^{\alpha\beta DC} \tag{11}$$

On the one hand, the zero sequence component of I_s can be considered zero due to the three wire connection[5]. On the other hand, the other DC components $I_s^{\alpha\beta DC}$ may circulate through the transformer windings leading to core saturation. Applying adequate differential voltage $v_{diff}^{\alpha\beta DC}$ values, these components can be regulated to zero.

An analogous procedure can be applied to the additive current of the converter. Therefore, applying (10) to (5), the DC components of the inner current can be expressed as

$$I_{sum}^{\alpha\beta DC} = -\frac{1}{2R_a} V_{sum}^{\alpha\beta DC} \tag{12}$$

and

$$I_{sum}^{0DC} = \frac{1}{2R_a}(V_t^{DC} - V_{sum}^{0DC}) \tag{13}$$

The zero sequence component of the additive DC current can be used to exchange power between the converter and the DC network and can be controlled applying additive DC voltage V_{sum}^{0DC}. On the other hand, $I_{sum}^{\alpha\beta DC}$ (circulating current) is controlled through $V_{sum}^{\alpha\beta DC}$ and can be used to exchange energy between the different legs of the converter to achieve internal energy balance. Thes components will be important under severe voltage unbalances in the AC network, as the power exchanged by the different legs will be significantly different.

[5] A different grounding scheme might change this conclusion.

1.3 MMC control requirements

The control strategy must be designed to meet several objectives:

- Control the different degrees of freedom of the MMC by means of specific current components
- Control the grid and additive currents flowing through the converter
- Establish a power exchange between the AC and the DC grid
- Continuous balancing of the energy stored in the converter arms, avoiding large deviations
- Enable the converter operation under any grid condition

To meet these objectives, the following parts of the control structure are addressed:

- Grid and additive current reference calculation considering unbalanced AC grid and DC voltage conditions
- Design of the grid and additive current regulators to track AC and DC current references
- Design of the energy regulators to balance the energy stored in the converter arms

Based on this structure a complete control scheme can be implemented as shown in Fig. 2 and Fig. 3. Next, the design of each part of the structure is discussed in detail.

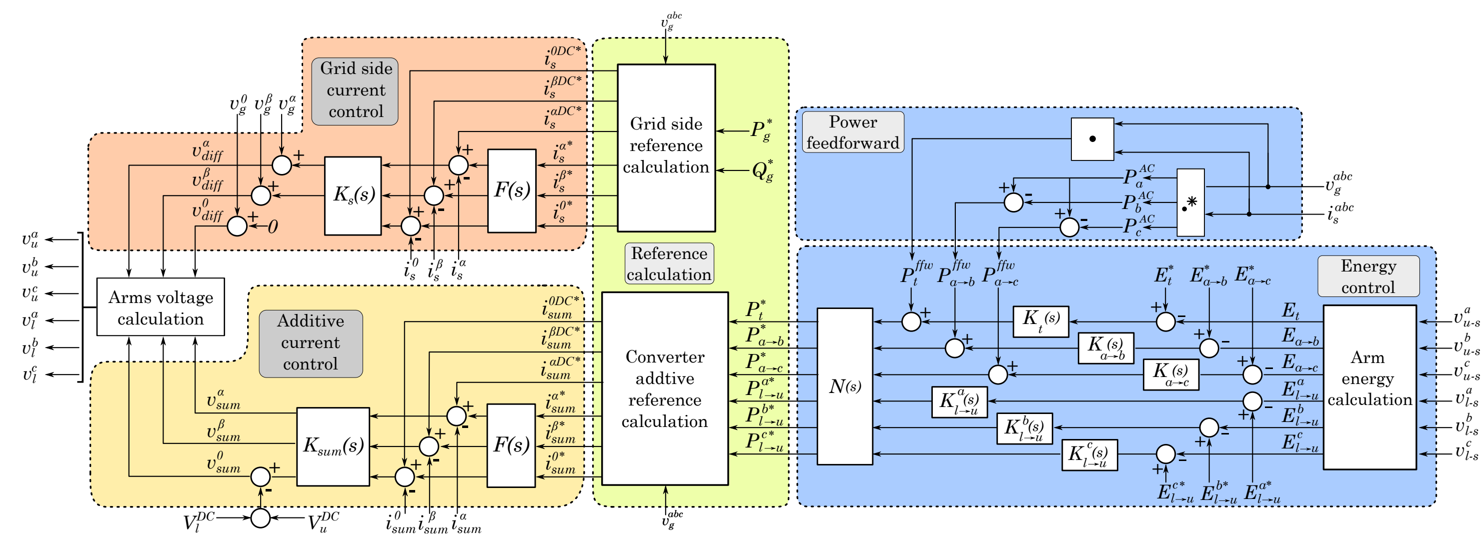

Figure 2: MMC control structure - Part I.

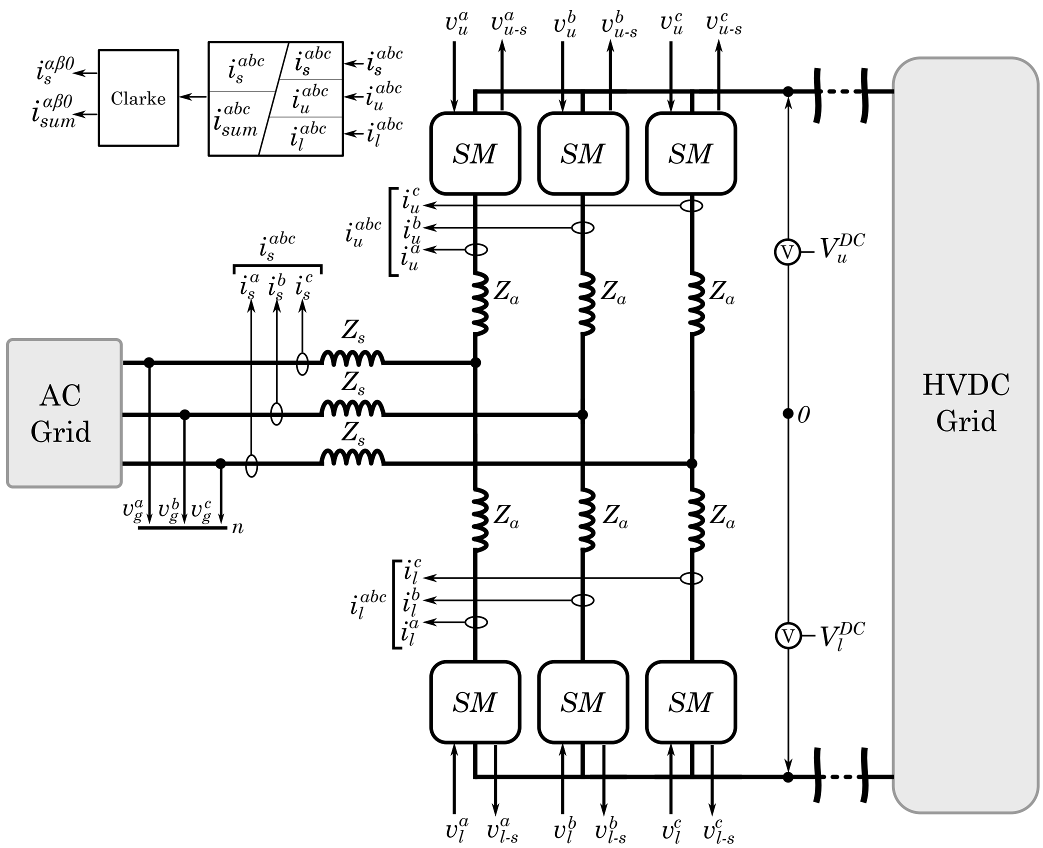

Figure 3: MMC control structure - Part II.

1.3.1 Current references calculation

As in most VSC topologies, the control structure for an MMC consists of a high-level power and energy controller which produces current reference values for a nested current controller, which in turn gives output voltage commands to a switching signal generator. Although the calculation of current reference values has elements in common with that of a two-level converter, the greater number of degrees of freedom of the MMC makes it of greater complexity.

1.3.1.1 AC network current references calculation

- DC component of the AC network current
  As discussed earlier, the zero sequence component of the AC network current is strictly zero due to the three-wire connection, and the reference of $I_s^{\alpha\beta DC}$ is set to zero and must be controlled to avoid transformer saturation.

- AC component of the AC network current
  The AC network current references can be calculated using the same methods as in classic two-level converters. Under balanced conditions, the two degrees of freedom of the current can be adjusted to obtain the desired active and reactive power exchange with the AC network [6]. However, when considering unbalanced AC network voltages several options exist [7], and the preferred solution has not been selected yet. The most common choice is to set the negative sequence current to zero and export only positive sequence current chosen to obtain the desired active and reactive power exchange. This causes an asymmetrical exchange of power between the AC network and the different legs of the converter even in steady state, which needs to be compensated by the converter to ensure internal energy balance. The calculation of the current reference is simplified by applying the so-called Park transformation matrix $\mathbf{T}(\theta)$ to voltage and current variables. The Park transformation is equivalent to the Clarke transformation combined with a rotation of angle θ and can be obtained as

$$\Theta^{qd0} = \underbrace{\mathbf{C}\,\mathbf{R}(\theta)}_{\mathbf{T}(\theta)}\,\Theta^{abc}; \quad \mathbf{R}(\theta) = \begin{bmatrix} \cos\theta & -\sin\theta & 0 \\ \sin\theta & \cos\theta & 0 \\ 0 & 0 & 1 \end{bmatrix} \tag{14}$$

  Following the nomenclature introduced by Akagi [6, 8], the non-oscillatory terms of the instantaneous active and reactive power of the power exported to the AC grid, P_g and Q_g respectively can be calculated from the positive voltage and current qd components as

$$P_g = \frac{3}{2}\left(v_g^{q+} i_s^{q+} + v_g^{d+} i_s^{d+}\right); \quad Q_g = \frac{3}{2}\left(v_g^{q+} i_s^{d+} - v_g^{d+} i_s^{q+}\right) \tag{15}$$

  Assuming v_g^{d+} to be zero, which can be granted if the angle of the Park transformation is chosen to match the angle of the positive sequence, the current references can be calculated as

$$i_s^{q^*} = \frac{2}{3}\frac{P_g^*}{v_g^{q+}}; \quad i_s^{d^*} = \frac{2}{3}\frac{Q_g^*}{v_g^{q+}} \tag{16}$$

This approach is sometimes known as the feed-forward method, as opposed to an alternative approach where the current reference is obtained from the output of a PI controller fed with the error between measured power and reference power. A discussion about their advantages and drawbacks can be found in [9]. If the converter is connected to a weak grid, the coupling between output current and grid voltage seen by the converter may require further consideration as shown in [10]. Finally, if the losses of the converter filter are not negligible, these can be included in the calculation of (16) for better accuracy [7].

1.3.1.2 Additive current references calculation

- DC component of the additive current
  The zero sequence component of the DC additive current I_{sum}^{0DC} is used to export power from the converter to the DC grid P_t, whereas the rest of the DC additive current is used to exchange power between converter legs $P_{a\to b}$ and $P_{a\to c}$. It is convenient to define the following new power variables

$$P_{a\to b} \triangleq P_a - P_b, \quad P_{a\to c} \triangleq P_a - P_c, \quad P_t \triangleq \sum_{j=a,b,c} P_j \tag{17}$$

where $P_j \approx V_t^{DC} i_{sum}^{jDC}$.

Similarly to the case of the AC network current, the approximation above assumes the losses of the arm inductors to be negligible. This enables calculating the current references in the Clarke reference frame as

$$\begin{bmatrix} i_{sum}^{\alpha DC^*} \\ i_{sum}^{\beta DC^*} \\ i_{sum}^{0DC^*} \end{bmatrix} = \frac{1}{3\,V_t^{DC}} \begin{bmatrix} 0 & 1 & 1 \\ 0 & \sqrt{3} & -\sqrt{3} \\ 1 & 0 & 0 \end{bmatrix} \begin{bmatrix} P_t^* \\ P_{a\to b}^* \\ P_{a\to c}^* \end{bmatrix} \tag{18}$$

Under normal operation, most of the DC additive current will be of the zero sequence component and it will be in charge of ensuring that the power exchanged between the converter and the AC network is equal to the power exchanged with the HVDC link. However, under severe voltage imbalances in the AC network, the DC additive current of phases a, b and c can be significantly different in order to compensate the power imbalance between phases.

- AC component of the additive current
  The AC voltage applied by the converter arms will be close to the AC network voltage. This can be seen from (8) given that $\underline{Z}$ is small. When comparing the AC voltage of the upper and the lower arms, they will have opposite signs. Therefore, the additive AC current $\underline{I}_{sum}^{+-}$ can be used to exchange power between the upper and lower arms of the converter. On the other hand, the zero sequence component $\underline{I}_{sum}^{0}$ must be set to zero to prevent AC current flowing to the HVDC link. Unlike the AC network current, the additive current can contain positive and negative sequence components with no impact on the AC grid. The power exchanged between upper and lower arms can be obtained by multiplying the AC arm voltage by the AC additive current. The AC arm voltage can be approximated as

$$v_l^{abc} \approx -v_u^{abc} \approx \sqrt{2}\begin{bmatrix} V_g^+\cos(\omega t) + V_g^-\cos(\omega t+\psi) \\ V_g^+\cos(\omega t - \frac{2\pi}{3}) + V_g^-\cos(\omega t+\psi+\frac{2\pi}{3}) \\ V_g^+\cos(\omega t + \frac{2\pi}{3}) + V_g^-\cos(\omega t+\psi-\frac{2\pi}{3}) \end{bmatrix} \tag{19}$$

  where ψ is the angle between the positive and the negative grid voltages. The AC additive current can be expressed as

$$i_{sum}^{abc} = \sqrt{2}\begin{bmatrix} I_{sum}^+\cos(\omega t+\gamma) + I_{sum}^-\cos(\omega t+\alpha) \\ I_{sum}^+\cos(\omega t+\gamma - \frac{2\pi}{3}) + I_{sum}^-\cos(\omega t+\alpha+\frac{2\pi}{3}) \\ I_{sum}^+\cos(\omega t+\gamma + \frac{2\pi}{3}) + I_{sum}^-\cos(\omega t+\alpha-\frac{2\pi}{3}) \end{bmatrix} \tag{20}$$

  where γ and α are the angles of the positive and negative sequence additive currents respectively, taking the positive sequence grid voltage as the reference of angles. Multiplying the arm voltages by the additive currents for phases a, b and c while eliminating the oscillatory terms at the double line frequency yields

$$P^a_{l\to u}(t) = V_g^- I^+_{sum} \cos(\gamma - \psi) + V_g^+ I^+_{sum} \cos\gamma + \\ V_g^- I^-_{sum} \cos(\psi - \alpha) + V_g^+ I^-_{sum} \cos\alpha \quad (21)$$

$$P^b_{l\to u}(t) = V_g^- I^+_{sum} \cos\left(\gamma - \psi - \frac{4\pi}{3}\right) + V_g^+ I^+_{sum} \cos(\gamma) + \\ V_g^- I^-_{sum} \cos(\psi - \alpha) + V_g^+ I^-_{sum} \cos\left(\alpha + \frac{4\pi}{3}\right) \quad (22)$$

$$P^c_{l\to u}(t) = V_g^- I^+_{sum} \cos\left(\gamma - \psi + \frac{4\pi}{3}\right) + V_g^+ I^+_{sum} \cos(\gamma) + \\ V_g^- I^-_{sum} \cos(\psi - \alpha) + V_g^+ I^-_{sum} \cos\left(\alpha - \frac{4\pi}{3}\right) \quad (23)$$

Note that there are four parameters that need to be chosen (I^+_{sum}, I^-_{sum}, α and γ) in order to adjust three power variables ($P^a_{l\to u}$, $P^b_{l\to u}$ and $P^c_{l\to u}$). The redundant degree of freedom can be used for secondary purposes such as minimizing losses. Here γ is chosen to be zero, thus the positive sequence current is chosen to be aligned with the positive sequence voltage. By introducing this condition, the former equations can be rewritten in a more compact form

$$\underbrace{\begin{bmatrix} P_1 \\ P_2 \\ P_3 \end{bmatrix}}_{P} = \underbrace{\begin{bmatrix} V_g^+ & 0 & V_g^- \cos\psi \\ 0 & V_g^+ & -V_g^- \sin\psi \\ V_g^- \cos\psi & -V_g^- \sin\psi & V_g^+ \end{bmatrix}}_{X} \underbrace{\begin{bmatrix} I^-_{sum} \cos\alpha \\ -I^-_{sum} \sin\alpha \\ I^+_{sum} \end{bmatrix}}_{I} \quad (24)$$

where the new power variables are defined as

$$\begin{aligned} P_1 &\triangleq \frac{1}{3}(-P^c_{l\to u} - P^b_{l\to u} + 2P^a_{l\to u}) \\ P_2 &\triangleq \frac{1}{3}(\sqrt{3}P^c_{l\to u} - \sqrt{3}P^b_{l\to u}) \\ P_3 &\triangleq \frac{1}{3}(P^a_{l\to u} + P^b_{l\to u} + P^c_{l\to u}) \end{aligned} \quad (25)$$

Based on the power references given by the energy controllers to maintain the energy balance between upper and lower arms, the current references can be obtained from (24) as

$$\underbrace{\begin{bmatrix} I_{sum}^{-}\cos\alpha \\ -I_{sum}^{-}\sin\alpha \\ I_{sum}^{+} \end{bmatrix}}_{I} = \underbrace{\frac{1}{(V_g^+)^2-(V_g^-)^2}\cdot\begin{bmatrix} M_{11} & M_{12} & M_{13} \\ M_{21} & M_{22} & M_{23} \\ M_{31} & M_{32} & M_{33} \end{bmatrix}}_{M} \underbrace{\begin{bmatrix} P_1 \\ P_2 \\ P_3 \end{bmatrix}}_{P} \tag{26}$$

$$M_{11} = \frac{2(V_g^+)^2 + (\cos(2\psi)-1)(V_g^-)^2}{2V_g^+}$$

$$M_{22} = \frac{2(V_g^+)^2 + (-\cos(2\psi)-1)(V_g^-)^2}{2V_g^+}$$

$$M_{12} = M_{21} = -\frac{\sin(2\psi)(V_g^-)^2}{2V_g^+}; \quad M_{33} = V_g^+$$

$$M_{13} = M_{31} = -\cos(\psi)V_g^-; \quad M_{23} = M_{32} = \sin(\psi)V_g^-$$

This equation has a discontinuity when $V_g^+ = V_g^-$, resulting in very high current reference values when voltage sags with high imbalance occur. One way to overcome this problem is to disable the AC component of the additive current upon detecting such disturbance and enabling it once the fault is cleared. Even though this makes the converter unable to control the balance between upper and lower arms during the sag, it is worth noting that there are no sources of sustained drift between upper and lower arms unless faults occur within the converter itself. Other possibilities have been studied in reference [2].

1.3.2 Current control

Note that all these equations are decoupled, therefore individual single-input single-output (SISO) controllers can be used for each of them. Different current control approaches can be implemented in order to meet the following requirements

- Perfect tracking simultaneously of AC and DC current components
- Tracking in the low milliseconds range
- Adequate positive and negative sequence components regulation

- Robust against harmonics and disturbances

To do so, several approaches can be followed:

- PI (DC) combined with resonant controllers (50 Hz)
- PI combined with prefilters to compensate the deviation at 50 Hz
- Advanced controllers (Fractional controllers, H-inf-based controllers, MIMO controllers, etc)

1.3.3 Energy Control

The energy regulators of the MMC set the references for the additive current controllers. There are six energy variables (one per arm) controlled by six different regulators. At this point, different strategies can be defined to maintain the internal energy balance [11]. One of these options consists on defining a new set of energy variables as

$$E_t = \sum_{j=a,b,c} E_u^j + \sum_{j=a,b,c} E_l^j \tag{27}$$

$$E_{a\to b} = (E_u^a + E_l^a) - (E_u^b + E_l^b) \tag{28}$$

$$E_{a\to c} = (E_u^a + E_l^a) - (E_u^c + E_l^c) \tag{29}$$

$$E_{l\to u}^j = E_l^j - E_u^j \tag{30}$$

where E_t is the total energy stored in the converter, $E_{a\to b}$ and $E_{a\to c}$ are the energy differences between legs a and b and a and c respectively, and $E_{l\to u}^j$ is the difference of energy between the upper and lower arms of leg j, with $j = a, b, c$. These are linear combinations of the total energy stored in the arms, which can be approximated as

$$E_u^j \approx \frac{1}{2}\frac{C_{module}}{N_{arm}}\left(v_{u-s}^j\right)^2; \quad E_l^j \approx \frac{1}{2}\frac{C_{module}}{N_{arm}}\left(v_{l-s}^j\right)^2 \tag{31}$$

where v_{u-s}^j and v_{l-s}^j are the sums of the capacitor voltages of all sub-modules of the upper and lower converter arms, respectively.

In order to achieve sustained operation, the energy stored in each of the arms should be equal. To do so, the energy differences between legs and between upper and lower arms must be regulated to zero while the total energy of the converter must be regulated to its rated value, given by

$$E_t^* = 6 \cdot \frac{1}{2} \frac{C_{module}}{N_{arm}} \left(V_t^{DC^*} \right)^2 \tag{32}$$

Clearly, additional energy control possibilities that handle the internal energy inside the converter can be implemented. However, the objective of maintaining the arms operating at the same energy level is common to all of them.

2 The DC/DC converter

The DC/DC converter for Direct Current (DC) grids is still a developing technology. The motivation of researching DC/DC converters for DC grids is the rapid growth of High Voltage DC (HVDC) transmission lines throughout Europe, China and other countries around the world. In the future, these point-to-point HVDC links can be interconnected to build a DC grid. Currently, HVDC links are designed to operate at different voltage levels, with different grounding configurations, and using different technologies (VSC or LCC). Therefore, in order to interconnect these HVDC links to form future DC grids, DC/DC converters are necessary.

In Deliverable 1.1, different DC/DC converter topologies for DC grids were discussed. This report focuses on one specific topology of DC/DC converter to illustrate the control requirements, protections and fault management of DC/DC converters. The mentioned topology focused on in this report is the Modular Multilevel Converter Dual Active Bridge (MMC-DAB). A MMC-DAB is built by interconnecting the AC terminals of two MMCs with an isolation transformer. It can be built either in single phase or three phase configuration, as shown in Fig. 4a and Fig. 4b.

2.1 DC/DC converter control requirements

In this case, the DC/DC converter control can be divided in two main parts, the control of the two MMCs and the power transfer between them to establish an adequate control for the DC network. Initially, the controller suggested in Section 1.3 can be adapted to be applied to control the two MMCs. Focusing on the DC/DC operation, the main control objectives are detailed:

- Control the different degrees of freedom of both MMC by means of specific current components
- Continuous balancing of the energy stored in the MMC, avoiding large deviations during operation
- Establish a power exchange between both MMC converters through the AC side (creating the AC network)

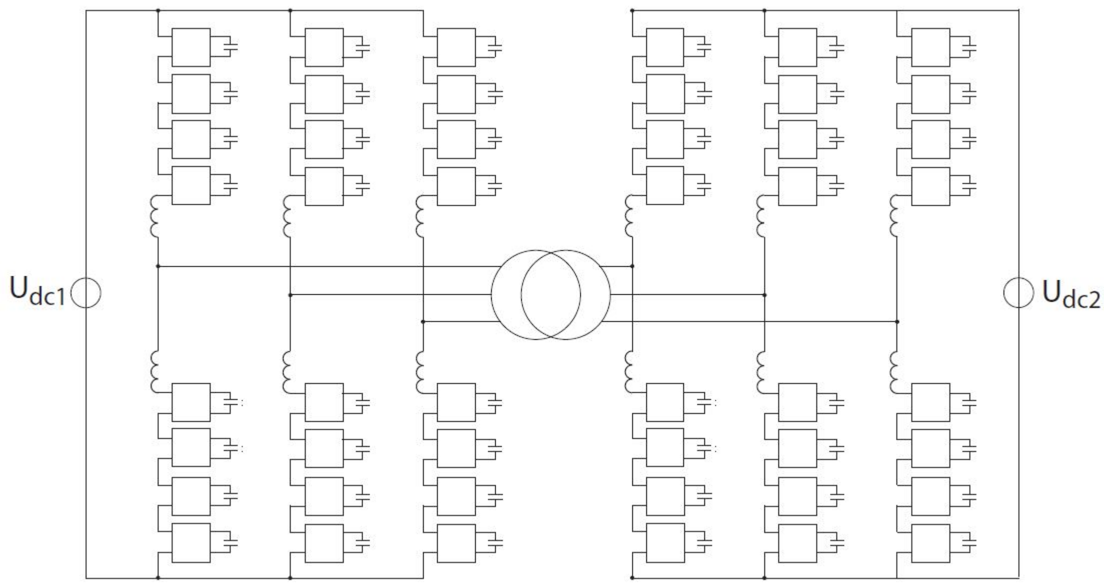

(a) Three-phase MMC-DAB DC/DC converter

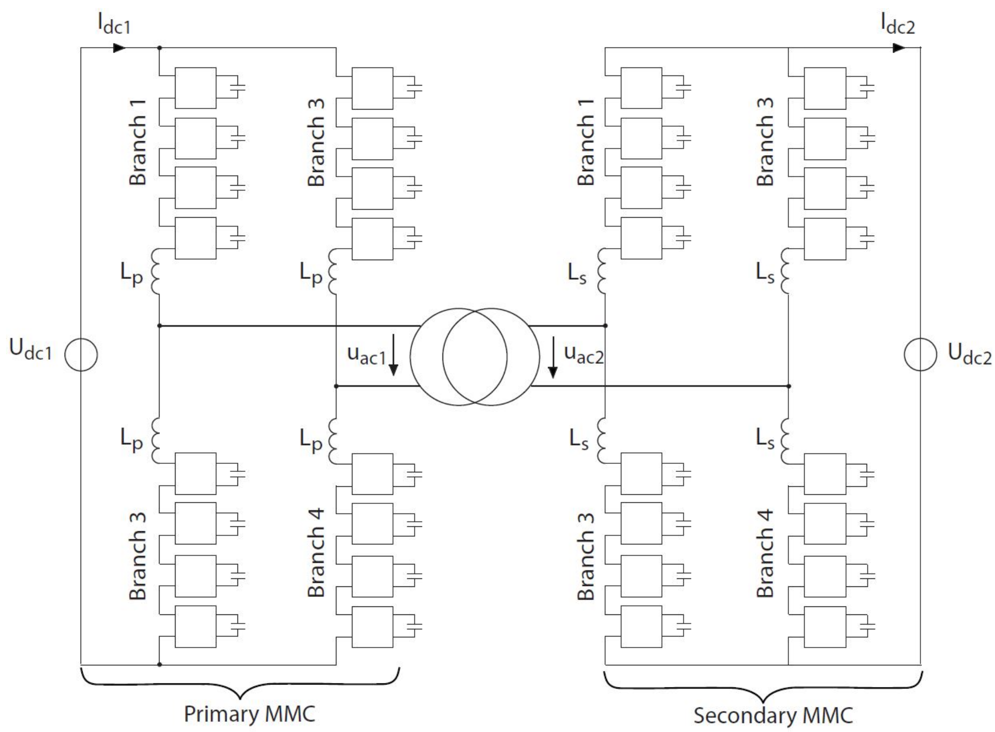

(b) Single-phase MMC-DAB DC/DC converter

Figure 4: MMC-DAB DC/DC converter [12].

- Establish an operation mode inside the DC network: DC power flow control or DC voltage regulation

The control structure suggested in [12] is used as a reference for the DC/DC control structure. As shown in Fig. 5, the control strategy consists of internal control and external control. The internal control focuses on the inner level MMC controllers including the arms and sub-modules balancing algorithms. On the other hand, the external control deals with the current/voltage regulation and the power flowing through the converter.

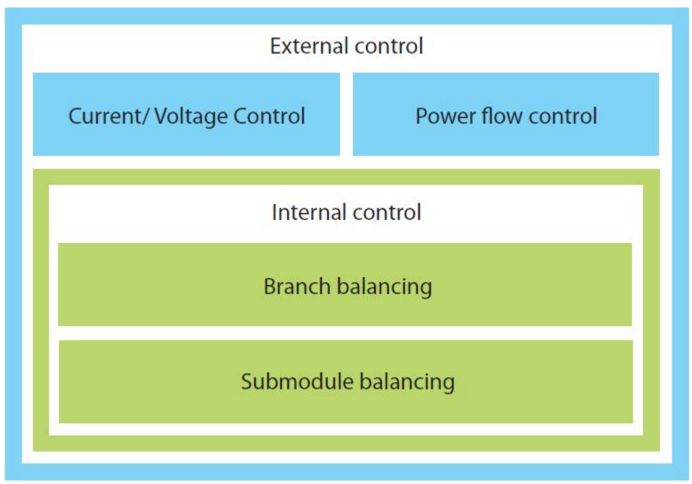

Figure 5: Hierarchical control of MMC-DAB [12].

2.1.1 Internal Control

The same energy balancing strategy for MMCs can also be used in MMC-DAB. Then, focusing on the capacitor balancing, a selection algorithm decides on which sub-module to be inserted or bypassed in order to balance the voltages on sub-module capacitors[6].

2.1.2 External Control

The power flow in MMC-DAB is managed by the phase-shifting angle between the voltage waveforms on the primary and secondary side of the transformer. The phase shift controller in Fig. 6 regulates the secondary DC

[6]Modulation strategies are expanded in appendix C

voltage by adjusting the phase angle of the voltage on the secondary side of the transformer, while the phase angle of the primary side voltage is fixed. Besires, additional controllers could be added to the external control layer to improve the performance of the converter.

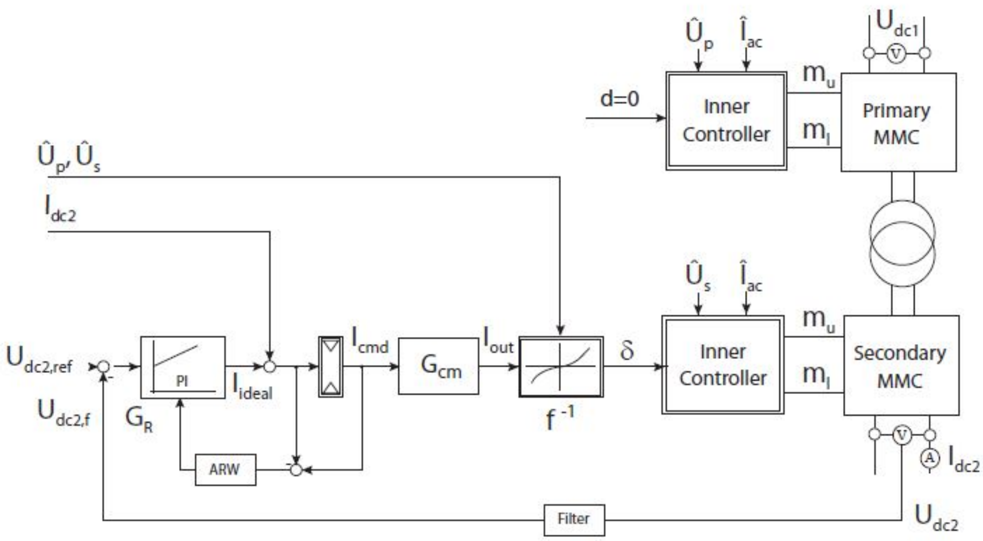

Figure 6: DC output voltage control of MMC-DAB [12].

2.2 Power flow control for MMC-DAB converter

Fig. 7 shows the phase-shift principle of MMC-DAB [13]. The two MMCs and the transformer in Fig. 4b can be simplified as two AC voltage sources and an inductor.

The power flow can be regulated by adjusting the phase-shift angle between two voltage sources. In a typical MMC application, the AC output should be modulated following a sine wave at 50/60 Hz. However, in MMC-DAB, since the AC link is just a middle transition stage, the frequency can be higher to reduce the size of the passive components in the converter, such as the transformer and the capacitors [14]. On the other hand, the increased frequency leads will raise the switching losses. In addition, there is no need to ensure strict sine waves for the MMC AC outputs. Both triangular and

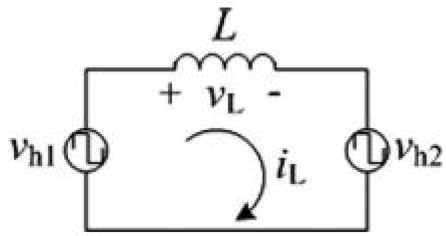

Figure 7: Simplified MMC-DAB circuit to design the power flow control [13].

square waves modulation could also be used. Different modulation strategies are detailed in the appendix C. Also, as an example of operation of the DAB DC/DC converter, appendix D experimental results have been included to illustrate its operation.

3 Protection and fault management of MMCs and DC/DC converters for HVDC

The main purpose of a protection system is to promptly remove any fault element from operation in order to preserve other components of the HVDC scheme from damages caused by the fault conditions. Furthermore, the protection system must be reliable and thus include autonomous supervision [15].

Next, the protections both for AC/DC and DC/DC converters operating in HVDC systems are described. It is assumed that the topology used in both cases is an MMC-based structure including half-bridge sub-modules.

3.1 AC faults operation

Prior to any control or protection action against a faulty condition, it is necessary to analyze the transient behavior of the fault. The control strategy detailed in Section 1.3 is able to handle converter transient AC unbalanced faults.

In Table 1, the classification of the different possible voltage sags is presented [16]. Two variables are used to describe the three-phase voltages during the sag: the pre-fault voltage E_1, and the voltage in the faulted phase (or between faulted phases) V. The impact of such faults in the MMC control can be summarized as:

- The converter phase-locked-loop (PLL) must be able to detect and separate positive and negative sequence
- Current controllers must be designed to track separately positive and negative sequence components
- Current reference calculation must be able to deal with unbalanced voltage conditions
- Converter energy is affected due to the unbalanced energy exchange per phase
- Energy regulators must ensure the stability of the converter

Simulations results are included in appendix B to illustrate the performance of the MMC converter during an AC fault.

Table 1: General classification of voltage sags

Type	Voltages	Phasors abc
A	$\underline{V}_g^a = V$ $\underline{V}_g^b = -\frac{1}{2}V - \frac{1}{2}jV\sqrt{3}$ $\underline{V}_g^c = -\frac{1}{2}V + \frac{1}{2}jV\sqrt{3}$	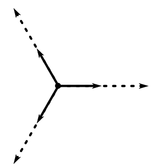
B	$\underline{V}_g^a = V$ $\underline{V}_g^b = -\frac{1}{2}E_1 - \frac{1}{2}jE_1\sqrt{3}$ $\underline{V}^c = -\frac{1}{2}E_1 + \frac{1}{2}jE_1\sqrt{3}$	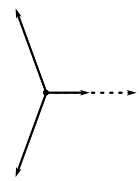
C	$\underline{V}_g^a = E_1$ $\underline{V}_g^b = -\frac{1}{2}E_1 - \frac{1}{2}jV\sqrt{3}$ $\underline{V}_g^c = -\frac{1}{2}E_1 + \frac{1}{2}jV\sqrt{3}$	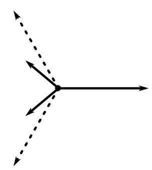
D	$\underline{V}_g^a = V$ $\underline{V}_g^b = -\frac{1}{2}V - \frac{1}{2}jE_1\sqrt{3}$ $\underline{V}_g^c = -\frac{1}{2}V + \frac{1}{2}jE_1\sqrt{3}$	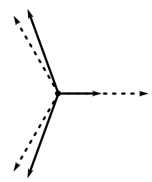
E	$\underline{V}_g^a = E_1$ $\underline{V}_g^b = -\frac{1}{2}V - \frac{1}{2}jV\sqrt{3}$ $\underline{V}_g^c = -\frac{1}{2}V + \frac{1}{2}jV\sqrt{3}$	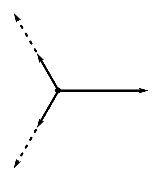
F	$\underline{V}_g^a = V$ $\underline{V}_g^b = -\frac{1}{2}V - \left(\frac{1}{3}E_1 + \frac{1}{6}V\right) j\sqrt{3}$ $\underline{V}_g^c = -\frac{1}{2}V + \left(\frac{1}{3}E_1 + \frac{1}{6}V\right) j\sqrt{3}$	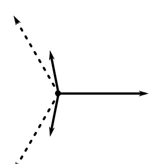
G	$\underline{V}_g^a = \frac{2}{3}E_1 + \frac{1}{3}V$ $\underline{V}_g^b = -\frac{1}{3}E_1 - \frac{1}{6}V - \frac{1}{2}jV\sqrt{3}$ $\underline{V}_g^c = -\frac{1}{3}E_1 - \frac{1}{6}V + \frac{1}{2}jV\sqrt{3}$	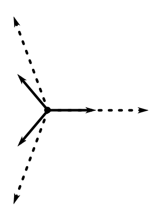

3.2 Protection system

According to [15], in operations whereby MMCs are used, the protection design must cover the following parts of the converter:

- Converter AC bus
- Converter DC bus
- Converter transformer (might be different in a DC/DC converter)
- Valve protection
- Phase reactor protection

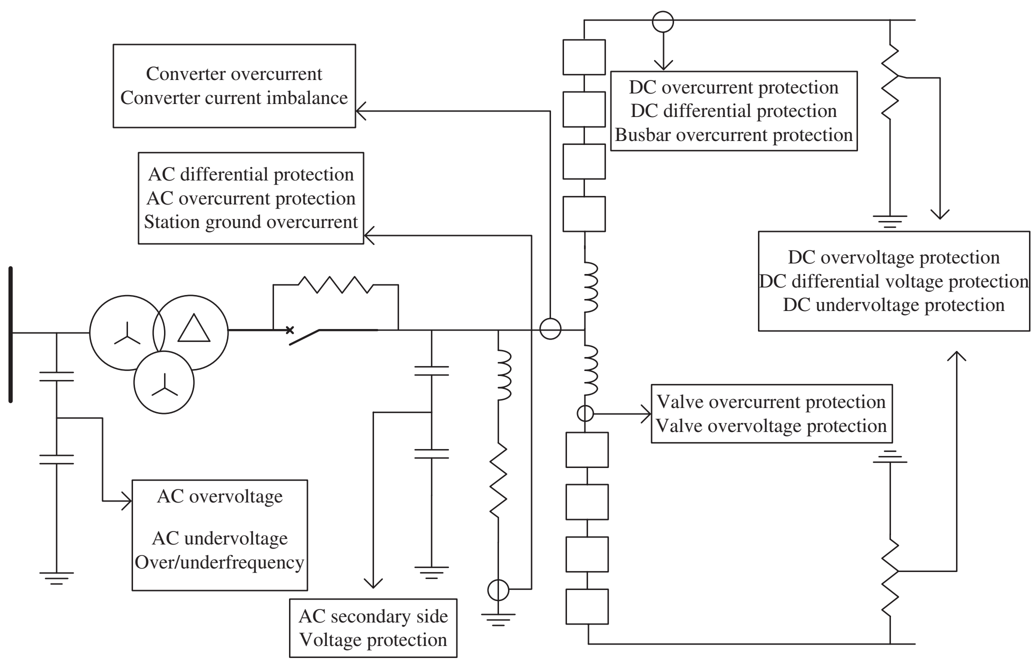

Figure 8: Typical protection system for MMC-HVDC [15].

3.2.1 AC side protections

For the AC side, the goal is to protect the converter against phase-to-phase or phase-to-ground faults. Typically, such faults can be handled by the control structure presented in the previous section. In cases where the control operation is not able to manage the fault, AC breakers are used to disconnect the converter [15]. To do so, several equipment are added to track the AC currents, voltages and frequency. Therefore, if the measurements present an abnormality, a signal will be generated and the AC breakers will be activated.

In a DC/DC converter structure, AC faults might happen inside the converter, thus alternative protection strategies might be required.

3.2.2 DC side protections

Due to the lack of reactors in the DC transmission line, DC faults can propagate faster than AC faults. Thus, the main goal of the DC protection system is to avoid overcurrent conditions [17]. Next, the protection management during different DC side faulty conditions is described. These protections can be applied both for an AC/DC and DC/DC topology.

- DC bus undervoltage and overvoltage protection
  The DC bus voltage is monitored and in case that it drops/increases to a certain level which is below/above the established threshold value, persisting for a defined period of time, the protection system will be activated blocking the converter [15].

  On top of the aforementioned, surge arresters can be added to the HVDC system to avoid overvoltages. They can be installed throughout the substation to protect different parts of the system.

  These elements are designed to behave as a small resistance when the ratio between the predefined overvoltage limit and the system operating voltage is greater than a set value. This ratio is called *switching surge factor* and it is generally set to be equal to 1.5 [18]. This value is obtained according to the substation specifications, and may vary depending on the scenario.

- DC link voltage unbalance protection
  The protection system measures the positive and negative pole voltages. The pole-to-ground voltage values are evaluated and in case of a difference greater than the predefined threshold level, the converter will stop operating.

- DC bus overcurrent protection
  The converter overcurrent protection shields the converter components (e.g. submodules and phase reactors) if abnormal overcurrent conditions are detected. If the current is greater than a threshold level for a predefined time, the converter is blocked.

- DC bus differential protection
  The DC bus differential protection keeps tracking the DC currents and in case of a large deviation between them, which indicates a severe fault condition, e.g. ground fault, the converter operation stops.

3.2.3 Valve and sub-module protection

Until now, the protection management systems were described for the AC and DC terminals. However, it is essential to analyze how the protection system can be implemented inside the Modular Multilevel Converter structure to avoid damaging the components within it.

Generally, MMC converters present several protection systems - overcurrent, overvoltage and undervoltage protections, which are located in the converter switches. During an abnormal condition, the protection system of the switches are activated, blocking and removing them from the circuit.

3.2.4 Transformer Protection

The primary objectives of the transformer protection are to protect the converter transformer from internal ground fault, phase-to-phase faults, and winding turn-to-turn faults. To do so, the transformers present several protection systems (e.g. overcurrent protection, differential protection between the primary and secondary windings, high temperature protection, and transformer gas detection and protection) [19] .

Typically, the primary and secondary side currents are compared considering the transformer turn ratio and tap position. If a discrepancy is detected in the fundamental current, the protection system is activated.

In addition, other protection systems for converter transformers are equipped with typical protective relays, such as:

- Buchholz relay

- Transformer winding temperature

- Tap changer pressure
- Transformer and tap changer low oil detector
- Transformer cooling system

3.3 SCADA Protection Functions for HVDC Grid

A technical report by National Grid suggests SCADA commands procedures in the Protection Functions, the commands follow the electrical, environmental and ancillary requirements in TS3.24.15 (RES), TS 2.19 (RES) and EATS48-4 [20, 21]. The protection functions of AC side and DC side are presented in the tables below. Starting from the AC Busbar in Table 2:

Table 2: AC Busbar Protection

AC Busbar Side	
Operational State	**Steps**
Double Busbar Arrangement	a) Trigger the converter blocking sequence b) Trip the main AC circuit breakers. c) Trigger circuit breaker failure, if available
Mesh Corner Arrangement	a) Trigger the converter blocking sequence b) Trip the related circuit breakers. c) Trigger circuit breaker failure protection, if available. d) Lockout Metering Communication and Data Acquisition Requirements. e) Trigger the right Direct Transfer Trip to the remote terminal units

Additional protection is monitored at the converter transformer Zone as shown in Table 3, [20, 21].

Table 3: Converter Transformer Protection

Converter Transformer Side	
Operational State	**Steps**
Tapping Sequence Protection	a) Trip tap-changer main circuit breakers b) Generate an alarm c) Block the converter if necessary

In the Converter side, many protection procedures are added and controlled by the SCADA system as shown in Table 4 [20, 21].

3.3.1 AC side protections

- Asymmetry protection
  This protection system detects any continuous presence of AC voltage components at 50/60 Hz, the 2nd harmonic component or current leakage between the DC terminals of the pole. The protection is activated when the the RMS magnitude of the AC components exceeds a pre-defined threshold.

- AC undervoltage protection
  The protection is blocked (trip the pole) when the voltage line-to-line drops below a threshold for a certain time.

- AC overvoltage protection
  The protection is activated only when a continued presence of overvoltage in the line winding side is detected for a certain time.

- AC overcurrent protection
  The protection detects overcurrents in the AC winding connections due to phase to phase valve connection faults or control failure

3.3.2 DC side protections

- Pole DC differential protection
  It is responsible of detecting the ground faults on the DC side of the converter. Normally, the procedure will take the pole out of service.

- DC overcurrent protection
  It detects overcurrent in the DC link and takes the pole out of service if triggered.

- DC undercurrent protection
  Detects open circuit operating conditions (e.g. de-block of one side of the converter). The protection aims to avoid one side of the converter (rectifier or inverter) from working if the other side is not responding (open circuit).

3.3.3 Differential protection

- AC>DC differential protection
  Responsible of monitoring the AC and DC currents. If an unexpected rise in the current of the AC leads to huge decrease in the DC currents due to a valve short circuit, then the pole should be taken out of service.

- DC>AC differential protection
  It is the opposite of the AC>DC and leads to eliminate the pole from service. This protection is activated when a converter failure leads to leakage current flow from the DC side to the AC side.

3.3.4 Valve protection

It is similar to the Line side Protection. However, it is measured using the transformer tap value (position). The characteristics of triggering the protection is defined by the valve surge arrester capability, and the AC filters voltage during any eventual tripping of the filters.

3.3.5 Transformer protection

Tap Limits Protection is responsible for limiting the impact of voltage fluctuation and stress on the converter equipment, e.g. over-excitation of the converter transformer.

Table 4: DC Converter/Pole Protection [20]

Converter/Pole Zone Protection	
Operational State	**Steps**
AC side protection (Asymmetry)	a) Initiate an alarm b) Shutdown the pole if the fault still exists
AC side protection (overvoltage, overcurrent)	a) Initiate converter blocking sequence b) Generate an alarm c) Trip the AC circuit breakers
side protection (undervoltage)	a) React with the relevant control functions b) Initiate converter blocking sequence c) Trip the AC circuit breakers d) Generate an alarm
DC side protection (pole DC differential protection)	a) Initiate converter blocking sequence b) Trip the AC circuit breakers c) Generate an alarm d) Isolate Line and Neutral
DC side protection (overcurrent)	a) Initiate converter blocking sequence b) Generate an alarm c) Trip the AC circuit breakers d) Isolate Line and Neutral
DC side protection (undercurrent)	a) Initiate converter blocking sequence b) Generate an alarm
Differential protection (AC>DC and DC>AC Differential)	a) Initiate converter blocking sequence b) Generate an alarm c) Trip the AC circuit breakers
Valve protection	a) Initiate converter blocking sequence b) Generate an alarm c) Trip the AC circuit breakers
Transformer protection	a) Generate an alarm b) Inhibit tapping to increase voltage c) Force tapping to Lower voltage

4 Conclusions

The operating principle of the MMC has been explained and its main mathematical model has been described. A steady state analysis is also included to illustrate the main degrees of freedom of the converter. Then, a control strategy is suggested to operate in normal operation and during unbalanced faults.

In addition, the control requirements and an example controller for an MMC-DAB DC/DC converter is described. Both simulation and experimental results of a two-level DAB are presented to verify the power flow control and voltage control of DAB.

Furthermore, MMC and DC/DC protection systems for HVDC applications have been introduced. The converter protection description has been divided between the AC and DC sides of the converter to provide a more comprehensive explanation.

A Modulation techniques for MMC

Different modulation techniques can be employed to drive MMC converters. However, the carrier-based PWM and the nearest level modulation (NLM) are the most used ones. Specifically, NLM or its variants are widely used in HVDC applications.

A.1 Carrier-based PWM

The carrier-based PWM strategy can be divided into three categories - level-shifted, hybrid carrier and phase shift PWMs.

Focusing on the phase-shift strategy, all the carriers have the same amplitude and offset, with a phase-shift of $2\pi/n$, as shown in Fig. 9. This method is advantageous due to the reduction of the dc-link capacitor voltage ripple and harmonic content reduction in the grid current [22]. For MMC applications, this modulation strategy can be used with limited bounds because it is unable to track drifts in the capacitor voltages [23].

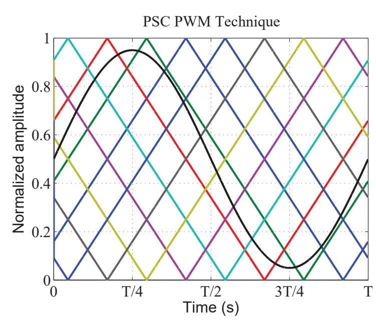

Figure 9: Phase-shift PWM strategy.

A.2 Nearest level modulation

The nearest level modulation (NLM) is a strategy in which the pulse patterns are added in order to create the desired number of submodules to be inserted or bypassed in the MMC, this set-point is obtained directly from the arm modulation index as m_{ul}^{abc*} [24]:

$$N_{ul}^{abc} = round(Nm_{ul}^{abc*}) \tag{33}$$

where N is the number of SMs available on the MMC stacks.

In this approach, the modulator (N_{ul}^{abc}) is discretized by rounding it to the closest integer number of SMs attainable, as seen in Fig. 10. The output waveform becomes closer to the real sinusoidal waveform as the number of levels increase [23].

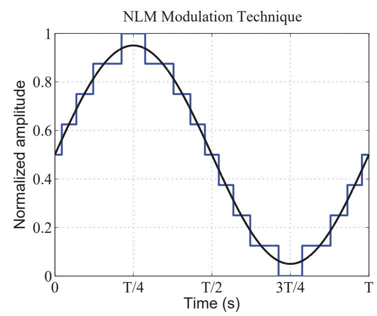

Figure 10: Nearest level modulation.

B Simulation of the MMC operation

In this section, two different simulations of the MMC are included to illustrate its operation. First, a simulation of the converter normal operation is explained showing the usual current and voltage transients during a power reference change. Then, the response of the MMC converter to an unbalanced AC voltage sag is detailed, showing that the converter is able to remain stable during and after the fault.

The MMC model used for the simulations is built based on the accelerated model proposed in [25, 26]. Each sub-module is represented by a capacitor that is charged or discharged depending on its switching state and the current that is flowing through its arm. The modulation technique implemented is the Nearest Level Control (NLC) technique [24]. The parameters of the simulation are included in Table 5.

B.1 Normal operation mode

Fig. 12 shows the converter response to a power reference set-point change from 0 to nominal power (injecting to the AC grid) at time 1 s. The power reference is changed following a first order system evolution with a settling time constant of 100 ms. A detailed legend for the color codes in Figs. 12, 13, 14 is shown in Fig. 11. It can be observed that the converter AC and DC power reach the steady state in the defined time. Fig. 12 confirms that the total sum of the energy of the arms is affected. However, the energy controller is able to compensate the effect without important deviations.

B.2 Unbalanced voltage sag

Fig. 13 and Fig. 14 show the converter response to an unbalanced type G voltage sag [16], with a positive sequence voltage of 0.5 pu and a negative sequence voltage of 0.25 pu. The voltage sag starts at time 3 s and the voltage is fully restored at time 5 s. The length of the sag has been extended to show the stability of the converter, whereas in a real system the sag condition would not be sustained further than 250 ms [27].

The control is set to inject only positive sequence current to the network while regulating the negative sequence to zero. It can be seen that the power exchanged by the converter has a double line frequency due to the unbalanced

Table 5: System parameters for an example MMC

Parameter	**Symbol**	**Value**	**Units**
Rated power	S	526	MVA
Rated power factor	$\cos\varphi$	0.95 (c)	-
AC-side voltage	U	320	kV rms ph-ph
HVDC link voltage	V_{DC}	$\pm$320	kV
Phase reactor impedance	Z_s	j 0.05	pu
Arm reactor impedance	Z_a	0.01+j 0.2	pu
Converter sub-modules per arm	N_{arm}	400	sub-modules
Average sub-module voltage	V_{module}	1.6	kV
Sub-module capacitance	C_{module}	8	mF

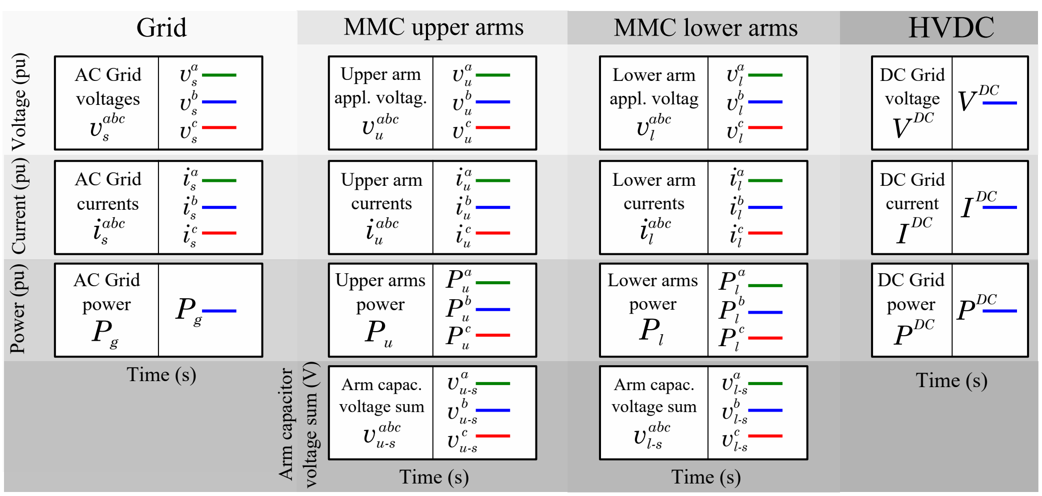

Figure 11: Graphs detailed legend for the simulation results.

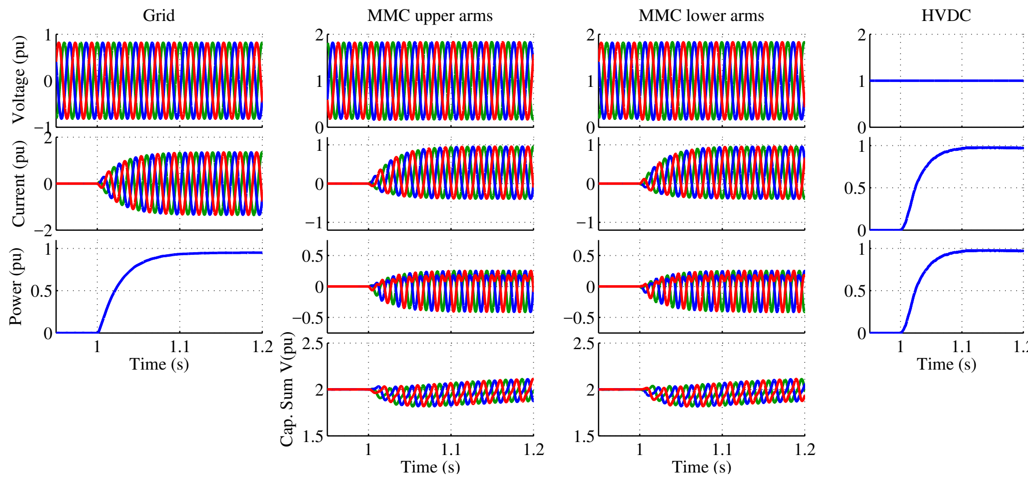

Figure 12: Simulation results of a nominal power step change

power exchange per phase. The active and reactive power management during the fault is following the grid code conditions [28]. It can be observed that the total sum of the capacitor voltages (converter energy) is affected by the voltage sag (see Fig. 13). However, the internal MMC controllers are able to regulate the converter energy back to their normal state. Finally, Fig. 14 shows how the converter goes back to its initial state upon clearing the fault without a significant deviation.

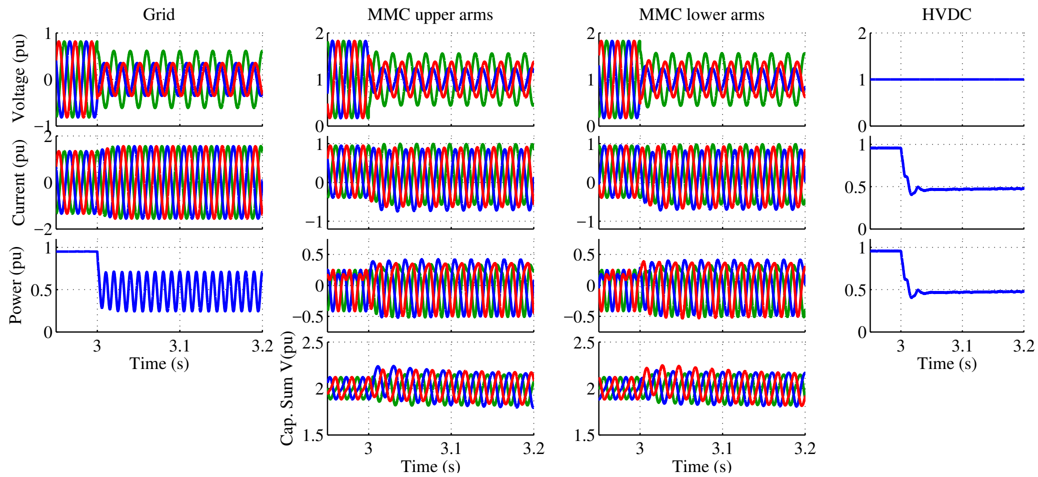

Figure 13: Simulation results of an asymmetrical voltage sag

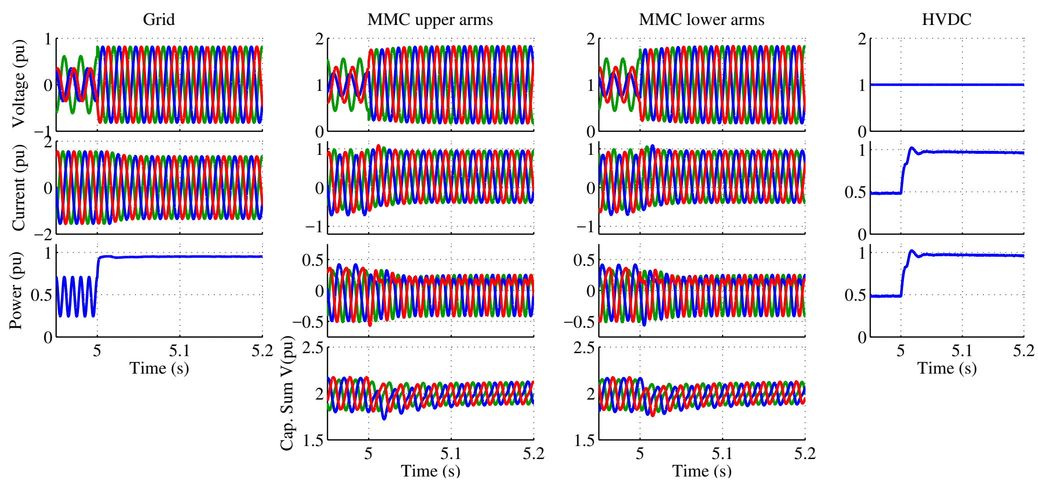

Figure 14: Simulation results of an asymmetrical voltage sag

C DC/DC Modulation Strategies

C.1 Sinusoidal Modulation

In [14], the sinusoidal modulation is used to operate the two MMCs in MMC-DAB to produce sinusoidal waveforms at 350 Hz. Both Carrier Phase Shift (CPS) SPWM and Nearest Level Modulation (NLM) can be used in MMC-DAB. As the AC link of the MMC-DAB is operated at a high frequency, and the switching frequency of CPS modulation will be tens of times higher than the operational frequency of the AC link, the fundamental wave modulation based on NLM is more preferable for the MMC-DAB to reduce switching losses, as shown in Fig. 15 [29].

C.2 Quasi Two-Level Modulation

Square wave modulation is widely used in two-level DAB as shown in Fig. 16 [31]. However, in MMC-DAB, ideal square wave modulation can not be realized due to the high voltage stress when all submodules in the same arm are simultaneously inserted or bypassed. Therefore, quasi two-level modulation is proposed in [32] to generate a quasi square wave from each MMC as shown in Fig. 17.

C.3 Triangular Modulation

As shown in Fig. 18, apart from the sinusoidal wave and quasi square wave techniques, a triangular wave can be used for modulation [30].

In [30], the above three modulation strategies are compared. The quasi two-level modulation has the highest power transfer ability, lowest sub-module capacitance requirement and lowest switching losses but highest circulating power. In addition, the voltage balance of the sub-module capacitors can be easily achieved with quasi two-level modulation. Overall, quasi two-level modulation is the best scheme for MMC-DAB to increase power transfer ability, power density and efficiency. Sinusoidal modulation has the lowest harmonic content so it is good for the high-frequency transformer, which can reduce the manufacturing difficulty of the high-voltage high-power high-frequency transformer. Comparing to quasi two-level modulation and sinusoidal modulation, triangular modulation has lower harmonics than quasi two-level modulation and a simpler algorithm than sinusoidal modulation.

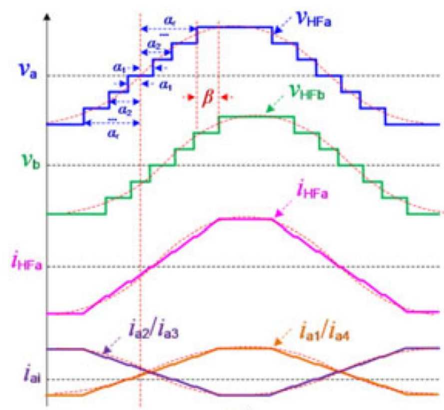

Figure 15: Sinusoidal modulation of MMC [30].

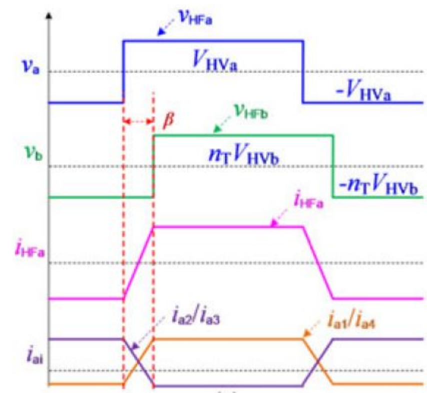

Figure 16: Square wave modulation of two-level DAB [31].

However, the triangular modulation scheme has the lowest voltage utilization and lowest power transfer ability.

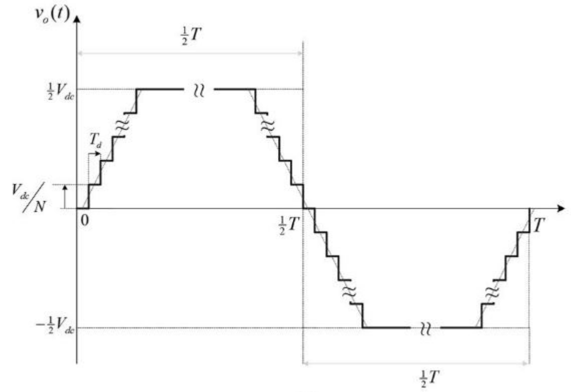

Figure 17: Quasi two-level modulation of MMC-DAB [32].

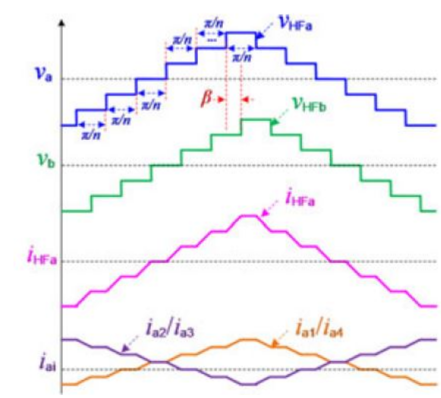

Figure 18: Triangular modulation of MMC-DAB [30].

D Simulation and Experimental results of DAB

A two-level DAB has been built both in a simulation and in an experimental setup to verify the control strategy shown in Fig. 6. The simulation model has been built in Matlab/Simulink as shown in Fig. 19. Simulation parameters are shown in Table 6. The simulation results of the two-level DAB are shown in Fig. 20. It can be seen that the AC output of both primary and secondary bridge are square waves at 20 kHz. The phase shift between primary and secondary voltages allows the power flows from the primary DC bus to the secondary DC bus.

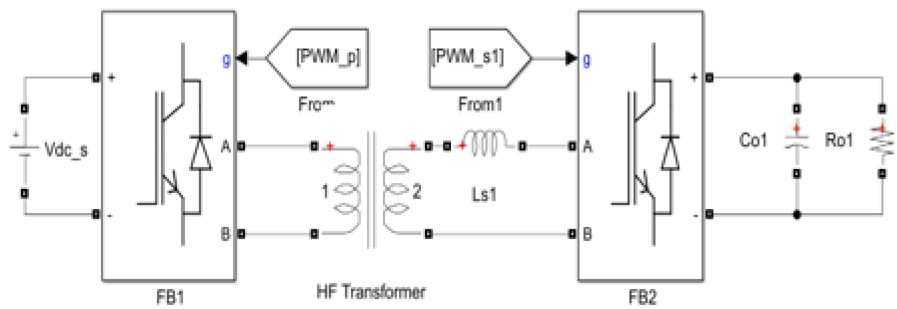

Figure 19: Simulation model of two-level DAB.

Table 6: Simulation parameters of two-level DAB.

Primary DC voltage	750 V	**Secondary DC voltage**	50 V
Secondary resistor	10 Ω	**Transformer winding ratio**	15 : 1
Switching frequency	20 kHz	**Modulation**	Square wave

The experimental platform of two-level DAB has also been built as shown in Fig. 21 and experimental results are shown in Fig. 22. The difference between experiment and simulation is that the primary DC voltage is set as 50 V and secondary voltage is controlled to be 10 V in the experiment. Further simulations and experiments will be developed during the duration of the project.

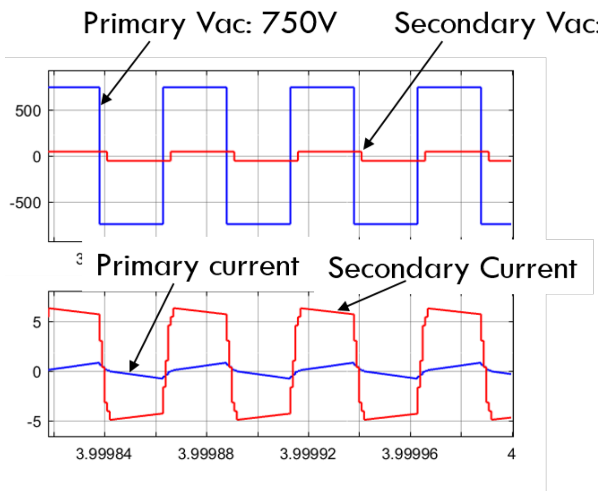

Figure 20: Simulation result of two-level DAB.

Figure 21: Experiment platform of two-level DAB.

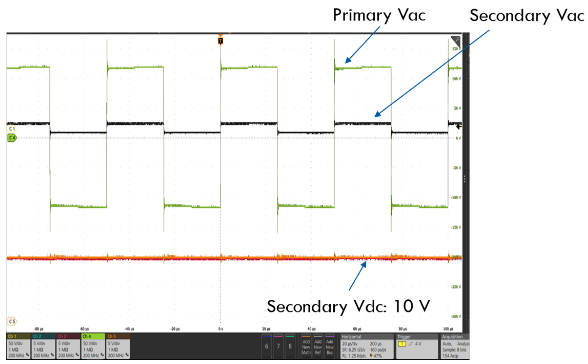

Figure 22: Experiment result of two-level DAB.

References

[1] Eduardo Prieto-Araujo, Adrià Junyent-Ferré, Carlos Collados-Rodríguez, Gerard Clariana-Colet, and Oriol Gomis-Bellmunt. Control design of modular multilevel converters in normal and ac fault conditions for hvdc grids. *Electric Power Systems Research*, 152:424 – 437, 2017.

[2] E. Prieto-Araujo, A. Junyent-Ferré, G. Clariana-Colet, and O. Gomis-Bellmunt. Control of modular multilevel converters under singular unbalanced voltage conditions with equal positive and negative sequence components. *IEEE Transactions on Power Systems*, 32(3):2131–2141, May 2017.

[3] Q. Tu, Z. Xu, and L. Xu. Reduced switching-frequency modulation and circulating current suppression for modular multilevel converters. *IEEE Transactions on Power Delivery*, 26(3):2009–2017, July 2011.

[4] S. Norrga, L. Ängquist, K. Ilves, L. Harnefors, and H. Nee. Decoupled steady-state model of the modular multilevel converter with half-bridge cells. In *6th IET International Conference on Power Electronics, Machines and Drives (PEMD 2012)*, pages 1–6, March 2012.

[5] C. L. Fortescue. Method of symmetrical co-ordinates applied to the solution of polyphase networks. *Transactions of the American Institute of Electrical Engineers*, XXXVII(2):1027–1140, July 1918.

[6] H. Akagi, Y. Kanazawa, and A. Nabae. Instantaneous reactive power compensators comprising switching devices without energy storage components. *IEEE Transactions on Industry Applications*, IA-20(3):625–630, May 1984.

[7] A. Junyent-Ferre, O. Gomis-Bellmunt, T. C. Green, and D. E. Soto-Sanchez. Current control reference calculation issues for the operation of renewable source grid interface vscs under unbalanced voltage sags. *IEEE Transactions on Power Electronics*, 26(12):3744–3753, Dec 2011.

[8] H. Akagi, E.H. Watanabe, and M. Aredes. *Instantaneous Power Theory and Applications to Power Conditioning*. IEEE Press Series on Power Engineering. Wiley, 2017.

[9] L. Shen, M. Barnes, R. Preece, J. V. Milanovic, K. Bell, and M. Belivanis. The effect of vsc-hvdc control on ac system electromechanical oscillations and dc system dynamics. *IEEE Transactions on Power Delivery*, 31(3):1085–1095, June 2016.

[10] A. Egea-Alvarez, S. Fekriasl, F. Hassan, and O. Gomis-Bellmunt. Advanced vector control for voltage source converters connected to weak grids. *IEEE Transactions on Power Systems*, 30(6):3072–3081, Nov 2015.

[11] S. Debnath, J. Qin, B. Bahrani, M. Saeedifard, and P. Barbosa. Operation, control, and applications of the modular multilevel converter: A review. *IEEE Transactions on Power Electronics*, 30(1):37–53, Jan 2015.

[12] K Stephan. *Modular DC/DC converter for DC distribution and collection networks*. PhD thesis, Ph. D. dissertation, EPFL, Lausanne, Switzerland, 2012.

[13] B. Zhao, Q. Yu, and W. Sun. Extended-phase-shift control of isolated bidirectional DC–dc converter for power distribution in microgrid. *IEEE Transactions on Power Electronics*, 27(11):4667–4680, November 2012.

[14] T. Lüth, M. M. C. Merlin, T. C. Green, F. Hassan, and C. D. Barker. High-frequency operation of a DC/AC/DC system for HVDC applications. *IEEE Transactions on Power Electronics*, 29(8):4107–4115, August 2014.

[15] Kamran Sharifabadi, Lennart Harnefors, Hans-Peter Nee, Staffan Norrga, and Remus Teodorescu. *Control and Protection of MMC HVDC under AC and DC Network Fault Contingencies*. IEEE, 2016.

[16] M.H.J. Bollen and L.D. Zhang. Different methods for classification of three-phase unbalanced voltage dips due to faults. *Electric Power Systems Research*, 66(1):59 – 69, 2003. Power Quality.

[17] Jianping Wang, Bertil Berggren, Kerstin Linden, and Reynaldo Nuqui. Multi-terminal dc system line protection requirement and high speed protection solutions. 2015.

[18] ORNL. HVDC power transmission technology assessment.

[19] Ieee guide for protecting power transformers. *IEEE Std C37.91-2008 (Revision of IEEE Std C37.91-2000)*, pages 1–139, May 2008.

[20] Protection & control for hvdc systems. Technical Report TS3.24.90 (RES) - Issue 1, National Grid, 2014.

[21] Ratings and requirements for plant, equipment and apparatus for the national grid system. Technical Report TS1 (RES) – Issue 1, National Grid, 2014.

[22] J. Holtz, W. Lotzkat, and K. . Werner. A high-power multitransistor-inverter uninterruptable power supply system. *IEEE Transactions on Power Electronics*, 3(3):278–285, July 1988.

[23] A. A. D. A. Ferreira. *Modular multilevel converters for power system applications*. PhD thesis, esi doctoral, UPC, Departament d'Enginyeria Elèctrica, 2017.

[24] Q. Tu and Z. Xu. Impact of sampling frequency on harmonic distortion for modular multilevel converter. *IEEE Transactions on Power Delivery*, 26(1):298–306, Jan 2011.

[25] Jianzhong Xu, Chengyong Zhao, Wenjing Liu, and Chunyi Guo. Accelerated model of modular multilevel converters in pscad/emtdc. *IEEE Trans. Power Del.*, 28(1):129–136, Jan 2013.

[26] A. Beddard, M. Barnes, and R. Preece. Comparison of detailed modeling techniques for mmc employed on vsc-hvdc schemes. *IEEE Trans. Power Del.*, 30(2):579–589, April 2015.

[27] ENTSO-E. Entso-E network code for requirements for grid connection applicable to all generators. Available at: https://www.entsoe.eu [accessed on February 2016]., 2013.

[28] *The Grid Code*. National Grid Electricity Transmission PLC, UK, 2015.

[29] P. M. Meshram and V. B. Borghate. A simplified nearest level control (nlc) voltage balancing method for modular multilevel converter (mmc). *IEEE Transactions on Power Electronics*, 30(1):450–462, January 2015.

[30] B. Zhao, Q. Song, J. Li, Y. Wang, and W. Liu. Modular multilevel high-frequency-link DC transformer based on dual active phase-shift principle for medium-voltage DC power distribution application. *IEEE Transactions on Power Electronics*, 32(3):1779–1791, March 2017.

[31] B. Zhao, Q. Song, W. Liu, and Y. Sun. Overview of dual-active-bridge isolated bidirectional DC–dc converter for high-frequency-link power-conversion system. *IEEE Transactions on Power Electronics*, 29(8):4091–4106, August 2014.

[32] I. A. Gowaid, G. P. Adam, A. M. Massoud, S. Ahmed, D. Holliday, and B. W. Williams. Quasi two-level operation of modular multilevel converter for use in a high-power DC transformer with DC fault isolation capability. *IEEE Transactions on Power Electronics*, 30(1):108–123, January 2015.

[33] L. Harnefors and H. . Nee. Model-based current control of ac machines using the internal model control method. *IEEE Transactions on Industry Applications*, 34(1):133–141, Jan 1998.

[34] Ian Postlethwaite. *Multivariable Feedback Control: Analysis and Design*. John Wiley & Sons, Inc., New York, NY, USA, 1996.

[35] H. Saad, X. Guillaud, J. Mahseredjian, S. Dennetière, and S. Nguefeu. Mmc capacitor voltage decoupling and balancing controls. *IEEE Transactions on Power Delivery*, 30(2):704–712, April 2015.

[36] L. Harnefors, A. Antonopoulos, S. Norrga, L. Angquist, and H. Nee. Dynamic analysis of modular multilevel converters. *IEEE Transactions on Industrial Electronics*, 60(7):2526–2537, July 2013.

[37] B. Zhao, Q. Song, J. Li, Y. Wang, and W. Liu. High-frequency-link modulation methodology of DC–dc transformer based on modular multilevel converter for HVDC application: Comprehensive analysis and experimental verification. *IEEE Transactions on Power Electronics*, 32(5):3413–3424, May 2017.

[38] Lennart Angquist, Antonios Antonopoulos, Daniel Siemaszko, Kalle Ilves, Michail Vasiladiotis, and Hans-Peter Nee. Open-loop control of modular multilevel converters using estimation of stored energy. *IEEE transactions on industry applications*, 47(6):2516–2524, 2011.

[39] Zhiwen Suo, Gengyin Li, Lie Xu, Rui Li, Weisheng Wang, and Yongning Chi. Hybrid modular multilevel converter based multi-terminal dc/dc converter with minimised full-bridge submodules ratio considering dc fault isolation. *IET Renewable Power Generation*, 10(10):1587–1596, 2016.

[40] Establishing a network code on requirements for grid connection of generators. *Official journal of the European Union*, (2016/631):L 112/1–L 112/68, April 2016.

[41] IEC. Surge arresters: Part 9: Metal-oxide surge arresters without gaps for HVDC converter stations 60099-9.